INFLUENCE OF THE STRESS RATIO ON THE VERY HIGH CYCLE FATIGUE BEHAVIOUR OF COMPOSITE MATERIALS

Martin Bartelt[1], Peter Horst[1] and Sebastian Heimbs[1]

[1] Institute of Aircraft Design and Lightweight Structures (IFL), TU Braunschweig, Germany,
martin.bartelt@tu-braunschweig.de, www.tu-braunschweig.de/ifl

Keywords: VHCF, Stress ratio, Cross-ply, Transverse cracking, Delamination

ABSTRACT

The very high cycle fatigue category stands for structural loading with up to 10^8 cycles. Testing in this region comes with multiple challenges like long testing times and self-fatigue of the test equipment. This results in a lack of research and leads to conservative designs of blades of wind turbines and helicopters.

The stress ratio is an important fatigue parameter and represents a missing piece in the very high cycle fatigue research puzzle. To investigate the influence of the stress ratio, four test series with two different cross-ply lay-ups made of glass fibres and epoxy resin are tested under alternating ($R = -1$) and swelling ($R = 0.1$) loads. The tests are conducted in a special very high cycle fatigue four-point bending test rig. The bending allows to investigate the separate effects of tension and compression on the front- and backside of the coupon-specimens from the swelling test series. The test rig is capable of in-situ recording of the flexural modulus. Also, the evolution of the two important fatigue damage parameters crack density and delamination area ratio are determined.

The first evaluations, studying the transmitted light photographs, already show for swelling loads higher fatigue limits on the tension side and no fatigue damages at all on the compression side, even at the highest tested load level. More detailed investigations, using the quantitative damage parameters, reveal lower crack densities and larger delamination areas per crack under swelling loading. Numerical calculations prove a shift of the dominant damage mechanism from transverse cracking to delamination, concerning the flexural modulus.

1 INTRODUCTION

Fatigue damage in fibre-reinforced plastics (FRP) is very different from fatigue damage in isotropic materials and requires a lot of research, due to its complexity. With the increasing use of FRP in high-performance structures, paired with the requirement of efficiency, the motivation of fatigue research up to very high load cycles rises.

Especially the very high cycle fatigue (VHCF) regime with up to 10^8 load cycles (LC) is underrepresented in research, mainly because of the high testing efforts. The main issues consist of long testing times (231 days for 10^8 LC at 5 Hz), specimen heating with higher testing frequency and self-fatigue of the test equipment. The missing research may prevent correct predictions of damage development and lifetime of highly fatigue loaded structures like rotor blades of wind turbines and helicopters as well as aircraft propellers [1, 2]. This leads to conservative and ineffective designs.

Existing research is mainly focused on determining SN-curves from total failure of specimens and fatigue limits, while the detailed damage phenomenology is mostly neglected. An overview regarding VHCF test methods and damage mechanisms is given by Shabani et al. [3].

One of the few research teams investigating the VHCF behaviour of quasi-isotropic and cross-ply carbon fibre reinforced plastics (CFRP) under tension loading in detail is the group of Hosoi et al. [4, 5, 6, 7, 8]. They determine damage parameters like the crack density and the delamination area ratio over the load cycles and address the damage phenomenology. Key insights are, first fatigue damage is nearly always transverse cracking, the existence of a lower transverse cracking threshold and contemporaneous delamination growth with the first transverse crack formation.

Further work on detailed damage phenomenology and basis for the investigations presented in this paper is conducted by Adam and Horst. They developed a four-point bending VHCF test system that overcomes the previously mentioned testing issues [9]. In tests on angle- and cross-ply glass fibre laminates the same damage mechanisms are recognised for low and high load cycle numbers. The damage development follows the known path of transverse crack initiation, -growth and –saturation, delamination growth and total failure (failure only in case of angle-ply laminates). The flexural modulus decline is supposed to be based mainly on the transverse cracking [10, 11, 12].

In general, it can be stated that the occurring types of fatigue damages, like transverse cracks and delamination, are the same from the low cycle fatigue (LCF) to the VHCF region [13, 14]. The difference between low and high load cycle regions merely lies in the interaction between fatigue damages, damage development, and fatigue limits.

Determining the role of the important fatigue loading parameter of stress ratio related to the mentioned aspects helps to partially complete the VHCF research gap. Investigations up to 10^7 load cycles already show higher degradations in terms of transverse cracking and shorter lifetimes under combined compression and tension loads compared to pure tension loading [15, 16, 17, 18]. Gamstedt and Sjogren [16] explain this phenomenon by additional fibre-matrix detachment due to compression loads leading to opening effects of the crack tip. The influence of the stress ratio on delamination growth has not yet been researched.

The first target of the conducted investigations is to verify, if the known effect of the stress ratio on transverse cracking and lifetime can be expanded into the VHCF regime under four-point bending. Furthermore, the determination of the effect on delamination growth is in focus.

To archive this, the four-point bending VHCF test rig is upgraded with the functionality of testing different stress ratios. This enables the testing of four test series (TS) with 0.5 mm and 0.25 mm transverse ply thickness under alternating (R = -1) and swelling (R = 0.1) loads. Multiple specimens are tested on one of up to seven load levels (LL) of every TS. The specimens are manufactured using the resin transfer moulding (RTM) process. Via the in-situ recorded flexural modulus, the crack density and the delamination area ratio development over the total fatigue test time of 10^8 LC, the effect of the stress ratio is determined in detail. The observed effects are verified by a parametric finite element model.

2 EXPERIMENTAL APPROACH

This study is part of a series of investigations covering the effects of different fibres [4], layer thickness, stress ratio and loading type, as well as fatigue limits on the VHCF behaviour of composite materials.

The specimens for the relevant TS 1 to 4 are manufactured from the same glass fibre / epoxy system and tested on the specialised VHCF four-point bending test rig. Except from the stress ratio and the lay-up (ply thickness) the experimental parameters stay the same for every specimen. Damages are evaluated by the flexural modulus and by the crack density and delamination area ratio which are derived from photographs by an in-house damage detection software.

2.1 Material and Specimens

The composite material used in the test series of this study consists of the glass fibre *SE2020* from *3B-fibreglas* and the epoxy resin system *RIM135R / RIM137H* from *Hexion*. According to the manufacturer, the fibre is optimised for fatigue using a special sizing. A comparison with another fibre and the same matrix reveals a strongly enhanced fibre-matrix adhesion, by an increase of the transverse strength of 122 % [19].

The first step of the composite manufacturing is the production of the fabric. To determine the undisturbed influence of the stress ratio, the fabric is produced by CNC-roving stacking without sewing threads. By using the RTM process for infiltration of the fabric with the RIM135 resin, the laminates are of high quality, with a smooth surface and high transparency. The specimens are cut out of the base laminate by CNC-milling. This ensures the correct laminate angle. To prevent crack initiation due to prior damages, the specimen sides are ground and polished. Figure 1 shows the geometric parameters of the specimens. The unidirectional (UD) mechanical properties of the SE2020 / RIM135 composite are listed in Table 1.

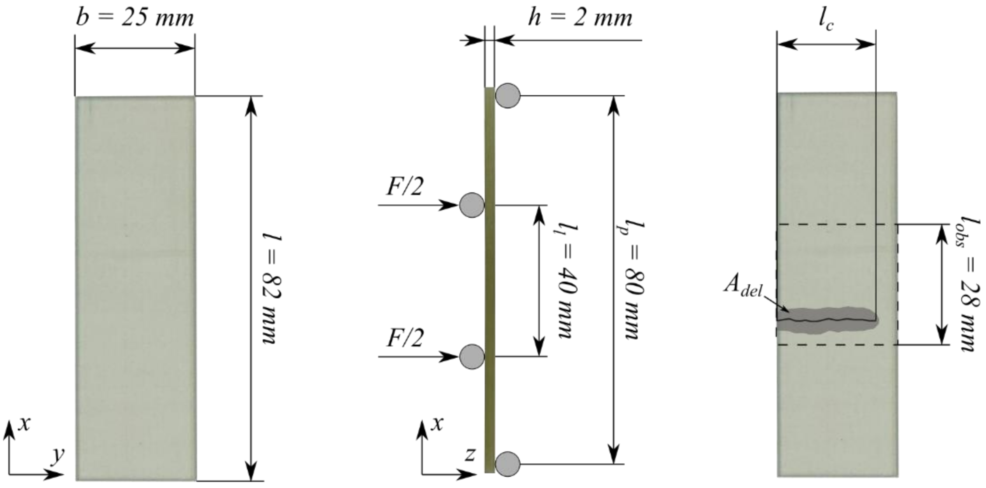

Figure 1: Geometric parameters of the specimens, the four-point bending device and the damage evaluation by Bartelt et al. [20].

Table 1: Tensile UD mechanical properties of the SE2020 / RIM135 composite from Chen [21].

Mech. Properties	*Unit*	*SE2020 / RIM135*
E_{11}	GPa	33.8
E_{22}	Gpa	7.8
R_{11}	Mpa	744
R_{22}	Mpa	60
ε_{11}	%	2.33
ε_{22}	%	1.1
φ_f	%	39.7

For the fatigue investigations, the two cross-ply lay-ups $(90_2/0_2)_s$ and $(90/0)_{2s}$ are manufactured and tested. The layer thicknesses of the outer 90°-layers, which are mainly loaded under bending, are 0.5 mm and 0.25 mm, respectively. To reach a layer thickness of 0.5 mm two layers of the 600 tex roving are stacked. In Figure 2 microscopic photographs of the two lay-ups are shown. The cross-ply lay-ups provide the advantage of low damage interaction compared to quasi-isotropic lay-ups. This enables an undisturbed determination of the influence of the stress ratio.

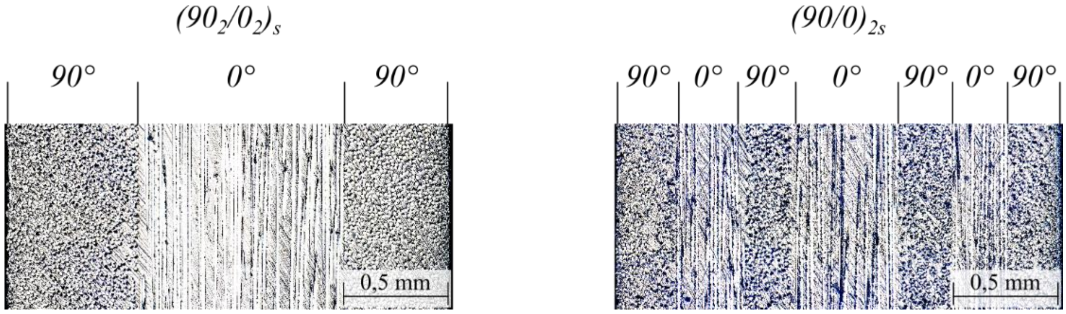

Figure 2: Microscopic photograph of the side of two specimens revealing the two lay-ups by Bartelt et al. [20].

2.2 VHCF Four-Point Bending Test System

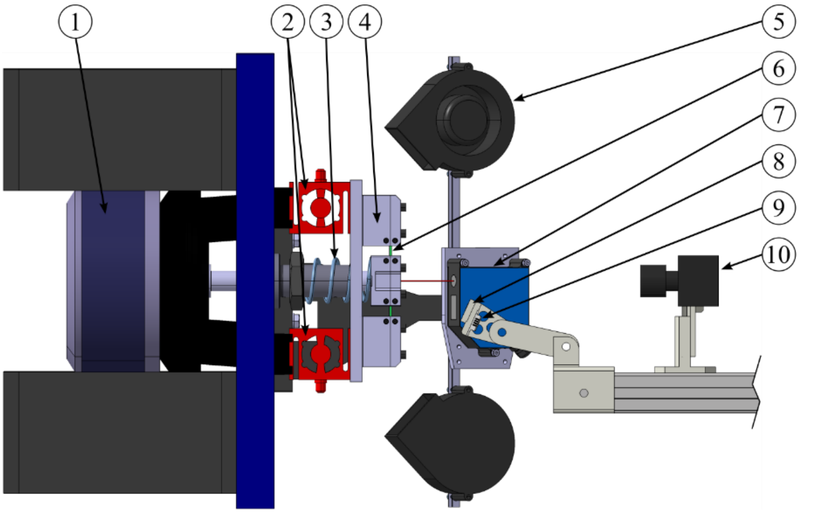

Figure 3: One of four test units of the VHCF test system by Bartelt et al. [20].

Common problems in VHCF testing are long testing times, self-fatigue and specimen heating at high testing frequencies. To overcome these problems, Adam and Horst [9] developed the specialised VHCF four-point bending test system, shown in Figure 3. The test system is further developed concerning an improved measurement accuracy and new features to enable the execution of this study.

One advantage of four-point bending compared to tension load is the lower required force to attain typical VHCF strain levels. These low forces can be reached using an electrodynamic actuator with lower self-fatigue, in contrast to typical hydraulic and mechanical actuators. The electrodynamic actuator is connected to the inner bearing of the four-point bending device. It deflects the specimen mounted between the inner and outer bearing with a frequency from 20 Hz to 80 Hz. Dimensions of the four-point bending device are given in Figure 1. Two load cells are mounted between the outer bearings and the base plate. Together with a laser triangulator the applied load and deflection of the specimen are recorded.

The external photo and infrared (IR) cameras are replaced during the upgrading of the test system with devices integrated in the control software (*NI LabVIEW*). The software automatically records photographs and the temperature distribution of the specimen. Also, the two cooling fans are controlled via the recorded temperature data.

An important feature added is the adjustable spring that is pushing against the inner bearing and applies a constant load. In combination with a constant current superimposed on the alternating load signal for the electrodynamic actuator, the test system is now capable of testing with an adjustable stress ratio.

Four identical units of the shown one are mounted on a damping concrete base and surrounded by a sound and thermal insulating housing, with a constant ambient temperature of 20°C.

2.3 Conducted Experiments

For this study, the four test series shown in Table 2 are conducted and evaluated. They differ in the layer thickness of the outer 90°-layer and the stress ratio. The influence of the stress ratio is determined by comparing TS1 with TS3, both having an outer layer thickness of 0.5 mm as well as TS2 with TS4 having a thickness of 0.25 mm. The influence of the layer thickness is already discussed by Bartelt et al. [20] and will be not be addressed in this study.

Every test series consists of up to seven load levels, defined by the surface strain of the outer 90°-layer at the beginning of the fatigue test $\varepsilon_{22,0}^{90^\circ}$. Multiple specimens are tested for every load level. The defining surface strain and the number of specimens per test series for the load levels are listed in Table 3.

Table 2: Fatigue testing parameters of the four test series.

Test Series	*Lay-up*	*Layer Thickness* t_{90}	*Stress Ratio* R
1	$(90_2/0_2)_s$	0.5	-1
2	$(90/0)_{2s}$	0.25	-1
3	$(90_2/0_2)_s$	0.5	0.1
4	$(90/0)_{2s}$	0.25	0.1

Table 3: Number of specimens tested per load level and test series.

Load level	*Surface strain* $\varepsilon_{22,0}^{90°}$	*Number of specimens* TS1	TS2	TS3	TS4
1	0.68	2	3	4	4
2	0.55	2	2	4	4
3	0.43	4	3	4	4
4	0.36	4	5	4	4
5	0.30	4	5		
6	0.25	4	4		
7	0.22	3			
	Total	23	22	16	16

The specimens are tested until 10^8 load cycles or until a high and constant damage state is reached. Reaching high and constant damage states already around 10^6 load cycles means per definition that the load level is in lower fatigue range than VHCF. This is the case for the LL1 and LL2 of the TS1 and TS2, which are classified into the high cycle fatigue (HCF) range. For reasons of phenomena comparison and relation of VHCF results these load levels are still useful.

With a testing frequency close to the natural frequency of the specimen and test system (50 Hz to 55 Hz) the test duration for one specimen is about four weeks.

The flexural modulus of every specimen is determined on a quasi-static four-point bending test stand before and after the fatigue test, to verify the flexural modulus measurement of the VHCF test system.

2.4 Damage Evaluation

One advantage of four-point bending over three-point bending is the constant bending moment between the two inner bearings, enabling a large observation area like it is shown in Figure 1 (right). By transmitted light photography the damages in this area are recorded. This is possible because of the high transparency of the laminate and a white led-screen mounted behind the specimen between the two inner bearings of the bending device (Figure 3).

Typical fatigue damages of cross-ply laminates under bending are transverse cracks and delaminations. The delaminations grow from the crack tip along the interface to the adjacent 0°-layer. These damages are quantified with the damage parameters crack density ρ and delamination area ratio H_{del}. The crack density

$$\rho = \frac{\sum_{i=0}^{n_c} l_{c,i}}{b_{obs} l_{obs}} \tag{1}$$

is defined by the sum of all crack lengths divided by the observation area. The width of the observation area b_{obs} is equivalent to the specimen width b. The length l_{obs} is given in Figure 1.

Similarly, the delamination area ratio

$$H_{del} = \frac{A_{del}}{b_{obs} l_{obs}} \tag{2}$$

is calculated with the delaminated area A_{del}. If fatigue damages occur on the front and back side of the specimen (relevant for $R = -1$), the damages from both sides are summed up and divided by twice the observation area.

Before the automation of specimen photography, around ten photographs were manually taken and evaluated per fatigue test. With the automation the density of data points is increased by taking 100 photographs per test. To reduce the evaluation work, an automated crack and delamination detection software is developed. This software is based on *Python* and *OpenCV*. It is validated with manually determined data.

The method of transmitted light photography comes with the possibility of a back side damage covered by a front side damage. In this case, the back side damage is not visible and hence not detectable manually or by the software. As the risk for low damage states is small, the method is valid for damage states typically reached in the VHCF range. For the HCF range the method may not be chosen, because of high crack densities and delaminations area ratios occurring.

As fatigue damage increases, the mechanical material parameters degrade. With the measurement of the force amplitude $\hat{F}$ and the deflection amplitude $\hat{w}_{max}$, the degradation of the simplified flexural modulus can be assessed by

$$\bar{E}_{x,b} = \frac{\hat{F}}{\hat{w}_{max}} \frac{(l_P - l_L)}{bh^3} \left(\frac{1}{4} (l_P - l_L)^2 + \frac{3}{4} l_L (l_P - l_L) + \frac{3}{8} {l_L}^2 \right) \tag{3}$$

using the inner and outer bearing distance l_L and l_P. The three damage parameters correspond to Adam et al. [10].

The lay-ups $(90_2/0_2)_s$ and $(90/0)_{2s}$ provide different flexural moduli before the fatigue test ($E_{x,b,0,0.5} \neq E_{x,b,0,0.25}$) and degrade to a different extent at same damage ratios. Therefore, a comparison of the mechanical degradation cannot be based solely on the flexural modulus of the total laminate. It must be based on the degradation of the outer 90°-layer. To specify this degradation, the ply discount value (PDV) is calculated. This value represents the flexural modulus of the lay-up without the outer 90°-layer on the tension side. The 90°-layer on the compression side is assumed to fully contribute to the flexural modulus, because damages on this side close under load and transfer forces. The PDV for the $(90_2/0_2)_s$-lay-up is $E_{x,b,pdv,0.5} = 0{,}641 \cdot E_{x,b,0,0.5}$ and for the $(90/0)_{2s}$-lay-up it is $E_{x,b,pdv,0.25} = 0{,}829 \cdot E_{x,b,0,0.25}$. Using the PDV, the degradation of the outer 90°-layer under tension can be calculated for a certain load cycle n by:

$$D^{90°}_{x,b,n} = \frac{E_{x,b,n} - E_{x,b,PDV}}{E_{x,b,0} - E_{x,b,PDV}}. \tag{4}$$

3 PARAMETRIC CRACK AND DELAMINATION SIMULATION MODEL

The experimental results are used to find phenomena related to the influence of the stress ratio. To understand the link between the stress ratio and its effect, a simulation of the relevant damage states can be helpful. Therefore, the parametric crack and delamination simulation model is developed. The overview of the model is shown in Figure 4. For the simulation environment *ANSYS* is chosen, and the code is written in *Ansys Parametric Design Language* (APDL). The following inputs are parameterised:

- the loading type (four-point bending / tension)
- the lay-up and material parameters
- the x-position of a variable number of cracks in the outer layer
- the length of delaminations at the crack tip along the layer interface

Basic simulation results are the displacement and the stress distribution. By using Solid 186 and Solid 187 elements, the calculation of the stress intensity factors at the crack tip is enabled. To reduce the calculation time, the specimen width of 25 mm is reduced to 4 mm. By comparing the results to analytical solutions, the model is validated.

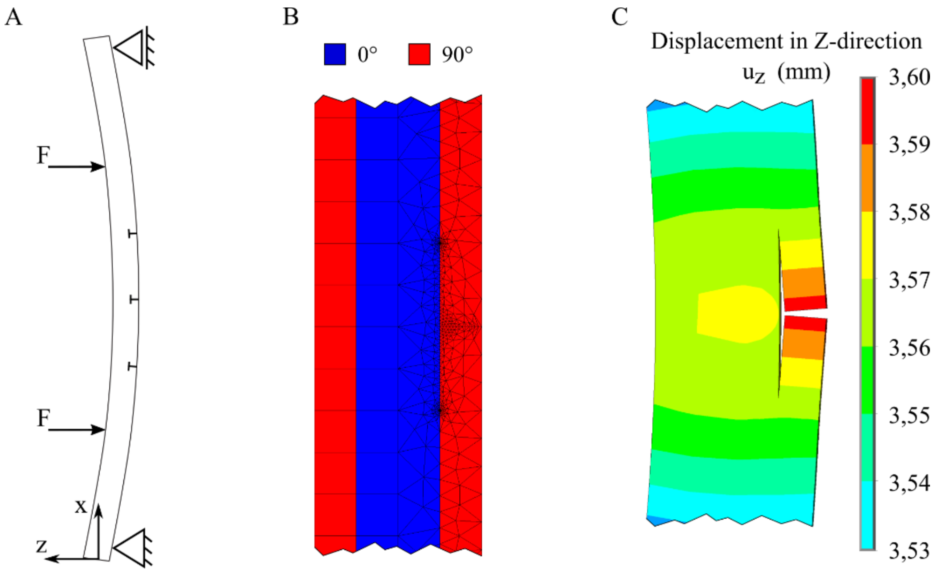

Figure 4: Numerical model overview: (A) Three cracks with delaminations simulated on the full specimen model, (B) close-up view of refined mesh and the lay-up at the centre crack, (C) displacement at the centre crack under LL3, by Bartelt et al. [20].

4 INFLUENCE OF THE STRESS RATIO

The fatigue test conditions, concerning stress states, the work done and the strain rate, vary with the stress ratio.

For alternating loads, the stress on both specimen sides switches between compression and tension. Swelling loads cause pure compression on one side and pure tension on the other side. Therefore, the fatigue results of the test series under swelling loads allow statements on compression and tension, at least until first damages occur and alter the stress state.

Also, it has to be mentioned that the work done and the strain rate under alternating loads are higher. The typical effect of a higher specimen temperature is reduced by the controlled cooling system, but other effects may apply.

The fatigue results are evaluated first by the photographic damage overview of every load level of the test series. In the following the quantitative damage parameters (see Chapter 2.4) are examined. The influence of the stress ratio is determined by comparing the test series 1 and 3 with 0.5 mm layer thickness of the outer 90°-layer and test series 2 and 4 with 0.25 mm layer thickness. Finally, the identified effects are assessed by simulating corresponding damage states in the parametric crack and delamination model.

4.1 Fatigue Results Overview

The fatigue damages of all test series are shown in the photographic overview in Figure 5 by one characteristic specimen per load level.

A first general observation is the increasing fatigue damage with the strain amplitude, from load levels without damage up to load levels with high damage states, for every test series. This indicates a valid fatigue testing and the correct choice of the load levels. The damage states within the load levels are consistent (not shown here), which also contributes to the validity of the tests.

The fatigue damages only occur in the outer 90°-layers. The inner 0°- and 90°-layers are free of any damage. Under lower loads typical weak spot cracking occurs, defined by irregular crack spacing. Regular crack spacing indicates the crack saturation state for accordingly higher loads.

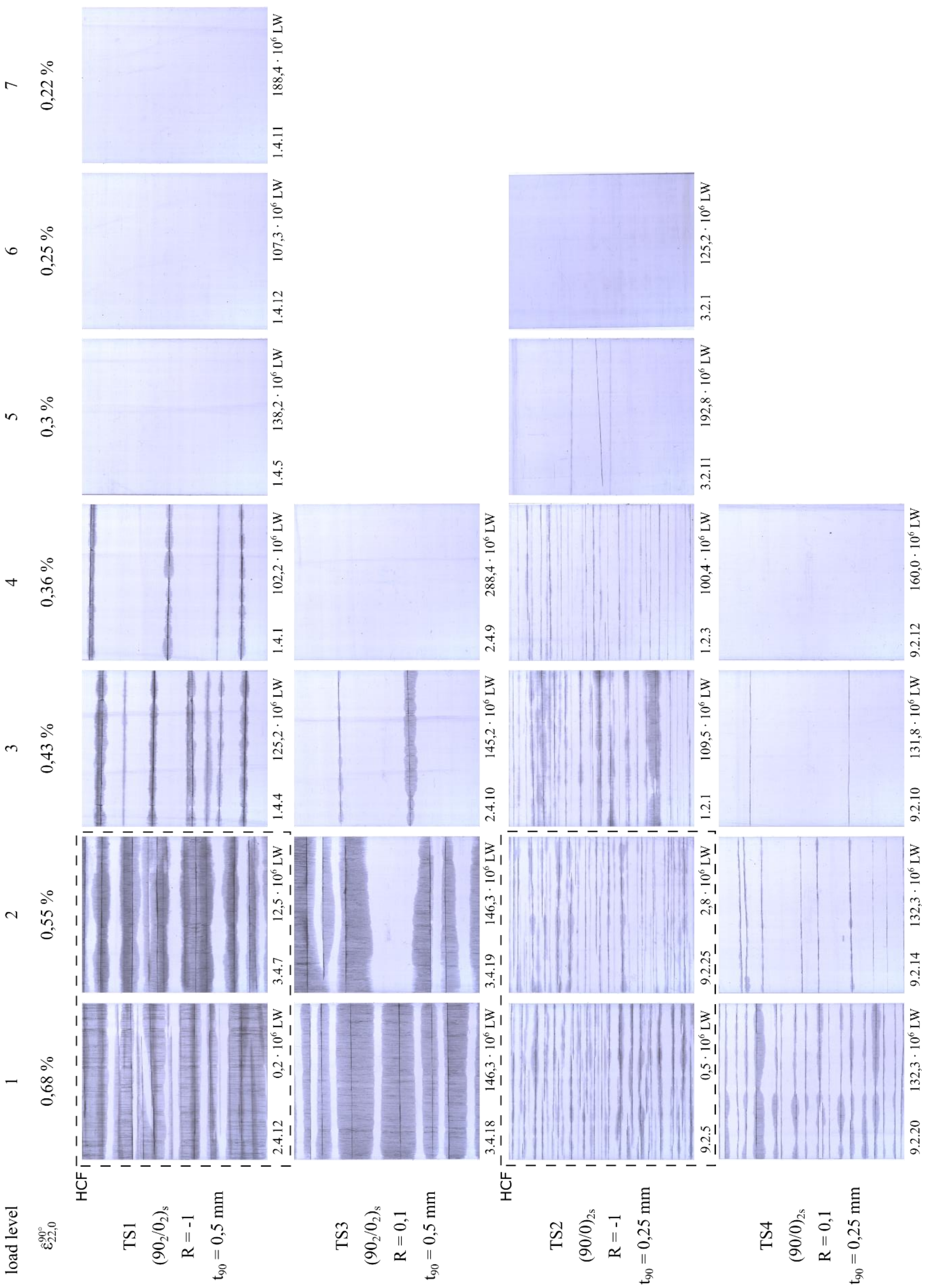

Figure 5: Overview of fatigue damage with one characteristic specimen for every test series and load level after the fatigue test.

The load levels 1 and 2 of test series 1 and 2 are classified as HCF, because of the high damage states reached after relatively low load cycle numbers. Also, the damage parameters are not evaluated, due to the high probability of overlapping damages on the front and back side.

Comparing the test series, the first visible effect of the stress ratio is a shift of the fatigue limit. Under alternating loads the limit is lower for both lay-ups with damage on both sides of the specimens. Under swelling loads damage only occurs on the tension side of the specimen. This holds true even for the highest load levels in this test campaign. This means a fatigue limit for compression loads is not reached in these tests.

Also, the damage states reached after 10^8 LC seem to be shifted in the same way as the fatigue limit. For a more detailed interpretation, the quantitative damage parameters are reviewed in the following.

4.2 Quantitative Damage Development

The damage parameters introduced in Section 2.4 are plotted over the load cycles for every test series in Figure 6. The flexural modulus degradation of the 90°-layer (top), the crack density (middle) and the delamination area ratio (bottom) of the specimens included in one load level are averaged. The standard deviation is given as grey area around the curves. Sudden changes of the curves are caused by the premature test ending of a specimen, like for LL3 of TS1 at around $88 \cdot 10^6$ LC.

The general observations like fatigue damage increase with the strain amplitude can be confirmed for all test series. The trend over the load cycles reveals a strong damage growth at the first $5 \cdot 10^6$ LC to $20 \cdot 10^6$ LC followed by a slow and steady increase until 10^8 LC for high loads. Accordingly, the degradation of the 90°-layer decreases strongly at the beginning and slowly towards the end. Very slow and no damage growth indicate the damage saturation state. The strong tendency of this material towards delamination, already investigated by Bartelt et al. [19], is recognisable by the synchronous crack and delamination growth.

In contrast to the degradation of the 90°-layer under high loads, the flexural modulus is rising under very low loads (LL6 and LL7) without any visible damages. This solidification is confirmed by accurate measurement of the specimen's flexural modulus before and after the fatigue test. The phenomenon is attributed to the alignment of the long-chain molecules of the polymer matrix.

The effect of the stress ratio concerning the aforementioned shift of damage states to higher loads under $R = 0.1$ is visible in the load level wise comparison of the test series. For example, LL3 leads to high crack densities under alternating loads (TS1: $\bar{\rho}_{90,LL3,max} = 0{,}21\ 1/mm$, TS2: $\bar{\rho}_{90,LL3,max} = 0{,}6\ 1/mm$) and lower ones under swelling loads (TS3: $\bar{\rho}_{90,LL3,max} = 0{,}04\ 1/mm$, TS4: $\bar{\rho}_{90,LL3,max} = 0{,}06\ 1/mm$). Similar damage states under swelling loads are reached under LL1 (TS3: $\bar{\rho}_{90,LL3,max} = 0{,}21\ 1/mm$, TS4: $\bar{\rho}_{90,LL3,max} = 0{,}5\ 1/mm$). This corresponds to a shift of approximately two load levels or 0.25 % of the initial surface strain amplitude.

Referring back to the fact of no damage initiation on the compression side of test series 3 and 4, but higher damage states reached under alternating compression-tension loads compared to swelling tension loads, it can be concluded that first damage is initiated by tension loads, before the compression loads contribute to the damage growth, like it is shown by Gamstedt and Sjogren [16].

Another important observation can be made for the ratio between the fatigue damage types of transverse cracks and delaminations. Especially for the $(90_2/0_2)_s$-lay-up the reached delamination area ratios are clearly higher at similar crack densities. For a crack density of $0{,}2\ 1/mm$ a delamination area ratio of 20 % (TS1, LL3) was reached under alternating loads compared to 70 % (TS3, LL1) under swelling loads. This means the stress ratio has an effect on the development of the damage path, according to the representation by Bartelt et al. [20] depicting the interaction between damages and their influence on crack initiation and delamination growth.

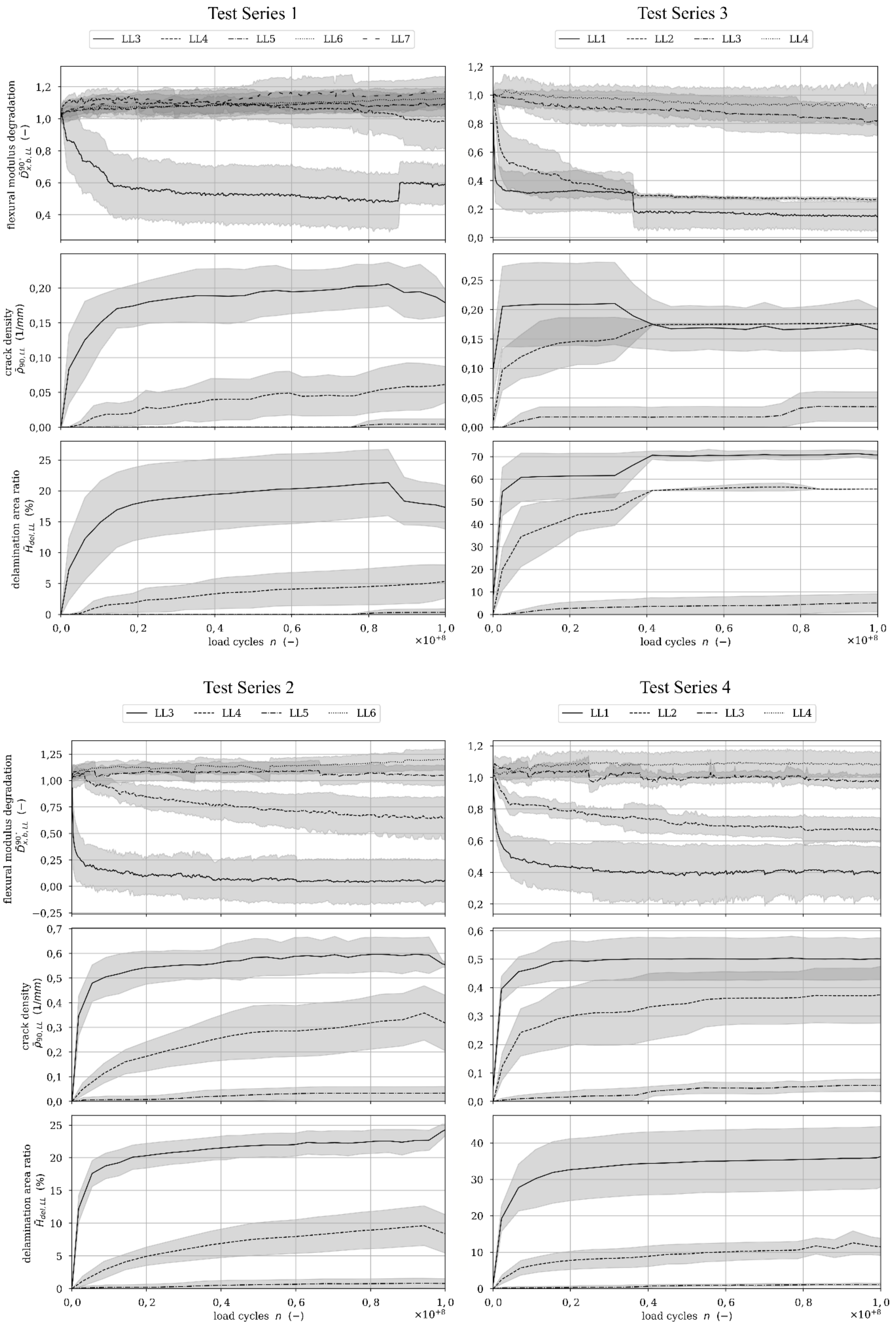

Figure 6: Development of the flexural modulus degradation, the crack density and the delamination area ratio, averaged over LL with standard deviation and smoothed for all TS.

It can be assumed that the missing compression load leads to the higher fatigue crack resistance under swelling loads, but the delaminations grow stronger under these high loads.

This raises the question, what impact the damage types have on the degradation of the mechanical material parameters? The strong degradation of the 90°-layer of TS3 – LL1 ($\overline{D}^{90°}_{x,b,LL1} > 80$ %) compared to TS1 – LL3 ($\overline{D}^{90°}_{x,b,LL3} \approx 50$ %) with a similar crack density shows the importance of this question, which will be investigated in the following using the parametric crack- and delamination model.

4.3 Numerical Investigation

To investigate the impact of transverse cracking and delamination on the mechanical material parameters, a specimen is simulated with different damage states under a certain load level. By using equation (4) the flexural modulus is calculated with the given geometry parameters, the applied force and the resulting deflection.

The first calculation is conducted with an undamaged specimen, to obtain a reference value of the flexural modulus. The impact of cracking is determined by the simulation of a single centred transverse crack without delaminations. By parametrically simulating evenly (idealised) growing delaminations from this crack, the degradation can be assigned to distinct delamination quantities. The delamination area per crack with the same degradation as caused by the single crack can be determined. This limit is then compared to the actual delamination area per crack of the fatigue test series. Therefore, the numerical calculations are conducted for both laminates. The results are listed in Table 4.

Table 4: Influence of the fatigue damage on the degradation of the flexural modulus determined from numerical simulations.

	$(90_2/0_2)_s$		$(90/0)_{2s}$	
Simulation	Flex. modulus $E_{x,b}$ (MPa)	Degradation $E_{x,b}/E_{x,b,0}$ (-)	Flex. modulus $E_{x,b}$ (MPa)	Degradation $E_{x,b}/E_{x,b,0}$ (-)
Undamaged ($E_{x,b,0}$)	12609		17667	
Single transverse crack with a total delaminated area of:				
0 mm^2	12355	0.9798	17585	0.9953
5 mm^2	12314	0.9766	17561	0.9940
10 mm^2	12276	0.9736	17538	0.9927
15 mm^2	12239	0.9706	17515	0.9914
17.7 mm^2 (interpolated)			<u>17504</u>	<u>0.9908</u>
20 mm^2	12199	0.9675	17492	0.9901
25 mm^2	12161	0.9645	17469	0.9888
30 mm^2	12121	0.9613	17445	0.9874
32.7 mm^2 (interpolated)	<u>12103</u>	<u>0.9598</u>		
35 mm^2	12082	0.9582	17422	0.9861

The data show that the same degradation by a single transverse crack and due to delaminations is reached at 32.7 mm^2 of delaminated area per crack for the $(90_2/0_2)_s$-laminate. For the laminate with the $(90/0)_{2s}$-lay-up, this limit is already reached at 17.7 mm^2 of delaminated area. This means, if the delaminated area per crack is higher in the respective test series, the delaminations take over the dominant share of flexural modulus degradation.

To compare these limits with the fatigue test data, the delaminated area per crack over the load cycles is calculated and given in Figure 6 for all load levels with fatigue damage. For the $(90_2/0_2)_s$-lay-up (top) all three load levels under swelling loads exceed the limit of 32.7 mm^2. With a thinner outer layer of 0.25 mm the reached delaminated areas under both stress ratios are lower. Only LL1 of TS4 reaches the

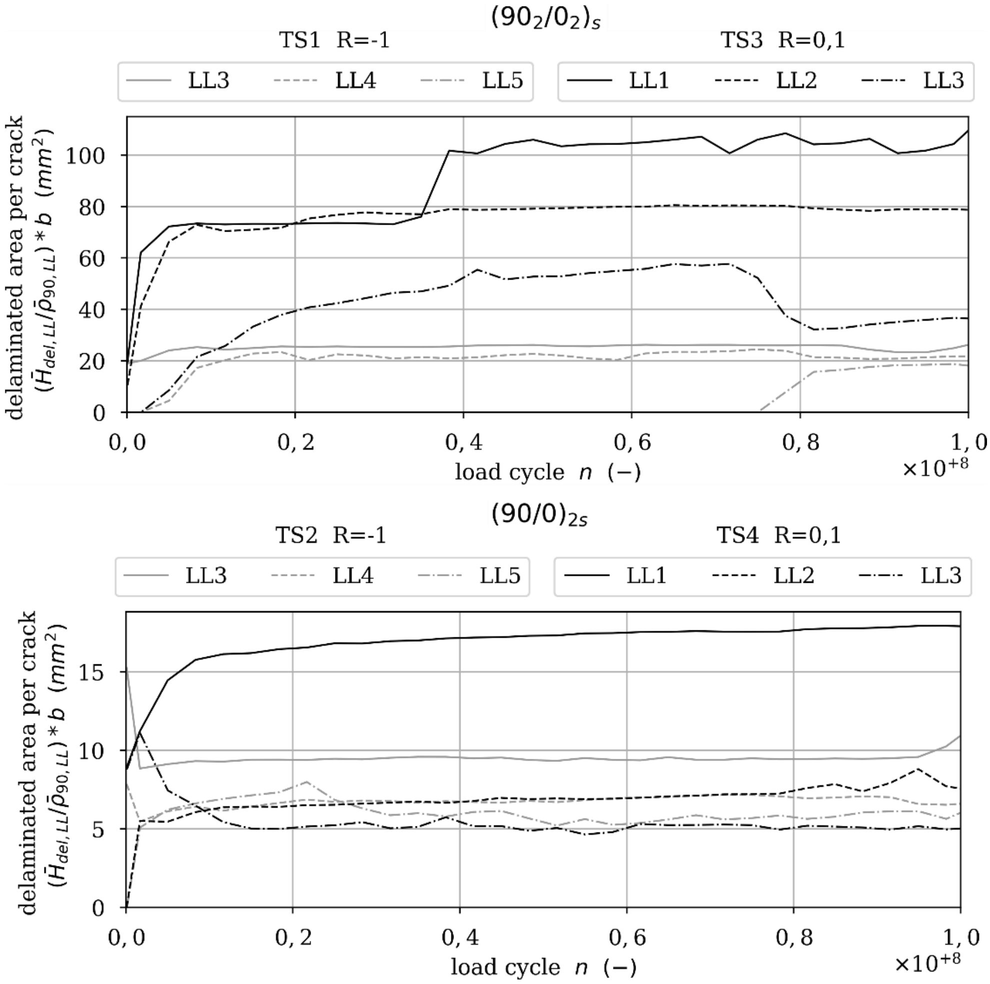

Figure 7: Development of the delaminated area per crack in comparison of the stress ratio for the $(90_2/0_2)_s$-lay-up (top) and the $(90/0)_{2s}$-lay-up (bottom).

limit, but does not exceed it significantly.

Finally, it can be stated that the dominant damage type changes from transverse cracking to delaminations for the 0.5 mm thick 90°-layers under swelling loading. This must be taken into account for fatigue-resistant design of structures with high performance laminates (high fibre-matrix adhesion [19]).

5 CONCLUSIONS

An extensive study in terms of quasi-static and fatigue testing and evaluating is conducted. The effect of the stress ratio is clearly visible and characterised for the VHCF regime for two laminates with different layer thicknesses.

For both laminates under swelling loads no damages at all were found on the compression side of the specimens. On the tension side a shift of the fatigue limit towards higher loads is recognised, compared to alternating loads. This can be referred to the findings of Gamstedt and Sjogren [16], showing the need of first micro fibre-matrix detachments due to tension, before compression takes a share on damage growth.

Also, high delamination area ratios under swelling loads were found and explained by a lower dependence of delamination growth on compression loading. By calculating the degradation effect of the crack density and delamination area on the bending modulus, it can be shown that the primary type of damage changes from cracks to delaminations for all load levels of the lay-up with 0.5 mm layer thickness. The change of the primary damage type is strongly recommended to be considered in the design process of fatigue-loaded structures.

ACKNOWLEDGEMENTS

The authors gratefully acknowledge the financial support of the German Research Foundation (DFG) within the project "Fatigue and fatigue limits in the VHFC regime of thin fibre-reinforced polymer laminates" under grant agreement HO2122/28-1.

REFERENCES

[1] J. F. Mandell and D. D. Samborsky, “DOE/MSU Composite Material Fatigue Database: Test Methods, Materials and Analysis,” *Contractor Report SAND97-3002 Montana State University,* 1997.

[2] J. C. Marin, A. Barroso, F. Paris and J. Canas, “Study of Fatigue Damage in Wind Turbine Blades,” *Engineering Failure Analysis,* vol. 16, no. 2, pp. 565–668, 2009.

[3] P. Shabani, F. Taheri-Behrooz, S. S. Samareh-Mousavi and M. M. Shokrieh, “Very High Cycle and Gigacycle Fatigue of Fiber-Reinforced Composites: A Review on Experimental Approaches and Fatigue Damage Mechanisms,” *Progress in Materials,* vol. 118:100762, 2021.

[4] A. Hosoi, J. Shi, N. Sato and H. Kawada, “Variations of Fatigue Damage Growth in Cross-Ply and Quasi-Isotropic laminates Under High-Cycle Fatigue Loading,” *Journal of Soild Mechanics and Materials Engineering,* vol. 3, no. 2, pp. 138-149, 2009.

[5] A. Hosoi, K. Takamura, N. Sato and H. Kawada, “Quantitative Evaluation of Fatigue Damage Growth in CFRP Laminates that Changes due to Applied Stress Level,” *International Journal of Fatigue,* vol. 33, pp. 781-787, 2010.

[6] A. Hosoi, S. Yagi, K. Nagata and H. Kawada, “Interaction between Transverse Cracks and Edge Delamination considering Free-Edge Effects in Composite Laminates,” *16th International Conference on Composite Materials,* 2007.

[7] A. Hosoi, Y. Arao, H. Karasawa and H. Kawada, “High-Cycle Fatigue Characteristics of Quasi-Isotropic CFRP Laminates,” *Advanced Composite Materials,* vol. 16, no. 2, pp. 151-166, 2007.

[8] A. Hosoi, Y. Arao and H. Kawada, “Transverse Crack Growth Behavior considering Free-Edge Effect in Quasi-Isotropic CFRP Laminates under High-Cycle Fatigue Loading,” *Composites Science and Technology,* pp. 1388-1393, 2007.

[9] T. J. Adam and P. Horst, “Very High Cycle Fatigue of Fibre-Reinforced Composites: An Alternative Experimental Approach,” *Proceedings of the 19th Int. Conference on Composite Materials, ICCM19, Montreal,* pp. 5012-5021, 2013.

[10] T. J. Adam and P. Horst, “Experimental Investigation of the Very High Cycle Fatigue of GFRP [90/0]s Cross Ply Specimens subjected to High-Frequency Four-Point Bending,” *Composites Science and Technology,* vol. 101, pp. 62-70, 2014.

[11] T. J. Adam and P. Horst, “Cracking and Delamination of Cross- and Angle-Ply GFRP Bending Specimens under Very High Cycle Fatigue Loading,” *Proceedings of the 20th Int. Conference on Composite Materials, ICCM20, Copenhagen,* 2015.

[12] T. J. Adam and P. Horst, “Fatigue Damage and Fatigue Limits of a GFRP Angle-Ply Laminate,” *International Journal of Fatigue*, 2017.

[13] R. Talreja, “Fatigue damage mechanisms,” *Modeling Damage, Fatigue and Failure of Composite Materials,* pp. 25-40, 2016.

[14] R. Talreja and C. V. Singh, “Damage and Failure of Composite Materials,” *Cambridge University Press,* 2012.

[15] H. El Kadi and F. Ellyin, “Effect of Stress Ratio on the Fatigue of Unidirectional Glass Fibre/Epoxy Composite Laminae,” *Composites,* vol. 25, no. 10, pp. 917-924, 1994.

[16] E. K. Gamstedt and B. A. Sjogren, “Micromechanics in Tension-Compression Fatigue of Composite Laminates Containing Transverse Plies,” *Composite Science and Technology,* vol. 59, no. 2, pp. 167-178, 1999.

[17] A. Rotem and H. G. Nelson, “Failure of a Laminated Composite under Tension Compression Fatigue Loading,” *Composites Science and technology,* vol. 36, no. 1, pp. 45-62, 1989.

[18] J. T. Ryder and E. K. Walker, “Fatigue of filamentary composite materials: Effect of compression on fatigue properties of a quasi-isotropic graphite/epoxy composite,” ASTM International, 1977.

[19] M. Bartelt, P. Horst and S. Heimbs, “Effects of an Enhanced Fibre-Matrix-Adhesion on the Fatigue Behavoiur of Composite Materials under VHCF,” *CEAS-Journal,* 2023.

[20] M. Bartelt, T. Luplow, P. Horst and S. Heimbs, “Influence of the Layer Thickness on the Very High Cycle Fatigue Behaviour of Composite Materials,” in *Proceedings of the 31st symposium of ICAF - the International Committee on Aeronautical Fatigue and Structural Integrity*, Delft, 2023.

[21] X. Chen, “Fabrication and Experimental Material Characterization of RIM135/SE2020 (600Tex),” Institut für Flugzeugbau und Leichtbau, TU Braunschweig, 2019.